

GT2011-45156

Studies on Two-Dimensional Contouring of High-Lift Turbine Airfoil Suction Surface as Separation-Control Device: Separation Suppression under Steady-State Flow Conditions

FUNAZAKI Ken-ichi, TANAKA Nozomi* and SHIBA Takahiro*

Department of Mechanical Engineering
 Iwate University
 Morioka, Japan

(* IHI Co. at present)

TANIMITSU Haruyuki and HAMABE Masaaki

Aerospace Operation
 IHI Co.
 Tokyo, Japan

ABSTRACT

The study the present authors have been working on is to develop a new method to increase aerodynamic loading of low-pressure turbine airfoils for modern aeroengines to a great extent, which is to achieve drastic reduction of their airfoil counts. For this purpose, this study proposes two-dimensional contouring of the airfoil suction surface as a device to suppress the separation bubble that causes large aerodynamic loss, especially at low Reynolds number condition. The main objective of this paper is to show how and to what extent the surface contouring without any other disturbances affects the suction surface boundary layer accompanying separation bubble. For comparison, rather conventional tripping wire technique is also employed as "local 2D surface contouring" to generate flow disturbances in order to suppress the separation bubble. All measurements are carried out under steady-state flow conditions with low freestream turbulence.

It turns out from the detailed experiments and LES analysis that the newly proposed two-dimensional contouring of the airfoil surface can effectively suppress the separation bubble, resulting in significant improvement of cascade aerodynamic performance.

NOMENCLATURE

C	: chord length
C_x	: axial chord length
C_p	: static pressure coefficient
d	: diameter of tripping wire
f	: frequency
k	: wave number
N_d, N_f	: data size, number of realizations
P_{01}, P_{02}	: inlet and outlet stagnation pressure
Re_2	: Reynolds numbers based on chord length and averaged exit velocity
RMS	: rms value of velocity fluctuation based on time-averaged velocity
RMS	: rms value of velocity fluctuation based on ensemble-averaged velocity
RRS	: reduction ratio of solidity
S_0	: total length of the suction surface

t	: airfoil pitch
Tu_{in}	: inlet turbulence intensity
U_{in}, \bar{U}_2	: inlet and averaged exit velocities
u_i, \tilde{u}	: instantaneous and ensemble-averaged velocities
x	: axial distance from the leading edge
Y_p	: stagnation pressure loss coefficient
y_n	: length along the normal direction to the surface
β_1, β_2	: inlet and outlet flow angles
σ	: solidity ($= C/t$)

SUBSCRIPT

1,2	: inlet, outlet
base	: base-type cascade
ref	: reference value
shear	: value associated with shear layer
x	: axial direction

ABBREVIATION

2D-C	: 2-dimensional contouring
HL	: High Lift (S-15)
UHL	: Ultra-High Lift (S-25)

1. INTRODUCTION

For modern commercial aeroengines, one of the key components to be developed further is highly-loaded but still efficient low-pressure turbine (LPT) airfoils, which could drastically reduce airfoil counts, eventually contributing to the development of lighter, more economical and greener aeroengines. Since such highly-loaded turbine airfoils usually suffer from the deterioration of aerodynamic efficiency, especially at cruise condition due to the occurrence of separation or separation bubble on the suction surface of the airfoil, a number of studies have been made on the development of new technologies to control the separation from various aspects, such as wake-separation interaction [1]-[4], free-stream turbulence [5]-[8], loading distribution [9]-[11], active control using plasma actuator [12]-[14] or jet [15]-[17]. Also, surface roughness, tripping wire and surface special treatment like dimple, groove or 2D/3D protrusion are rather conventional but still attracting

attention from researchers and designers [18]-[22]. Luo et al. [21] carried out LES (Large-Eddy Simulation) analysis to examine how surface treatment with spanwise (2 dimensional) groove on a highly loaded LP turbine airfoil affected the separation bubble. They suggested that the groove can change the instability mechanism, which prompts transition inception of the separation bubble, although no experimental evidence was shown there. Martinstetter et al. [23] invented a new type of turbulator on the airfoil suction surface, so-called T.ISA, and executed experimental investigation on how this turbulator worked as separation-controlling device under several steady and unsteady flow conditions. The design concept of the turbulator was to induce a horseshoe vortex which only modifies the instability characteristics of the boundary layer with separation slightly, rather than forcing its abrupt transition. They revealed that the turbulator exhibited a favorable performance in suppressing separation bubble suppression or reducing cascade loss under both steady and unsteady flow conditions for the wide range of Reynolds numbers, although the adopted wake passing Strouhal number, which specifies the unsteady flow condition, was considerably low compared to that of design condition. Unfortunately, no detailed flow measurements over the suction surface were made in their study, therefore, important information on time-averaged as well as time-resolved pictures of the flow over the surface is lacking and no explanation is available on the mechanism of the separation suppression.

The authors propose a new type of separation-controlling device on highly-loaded low-pressure turbine airfoils for modern aeroengines in this study. The device is created by modifying the front half of the suction surface of the original airfoil into a kind of back-facing small step with gradual slope at the windward side, which can be regarded as two-dimensional (2D) contouring of the surface. The concept of this surface modification (contouring) is to generate turbulence flow with moderate intensity before the separation bubble with no structural and manufacturing penalties associated with the application of the modification. For the sake of comparison, airfoils with tripping wire embedded along with the spanwise direction on the suction surface, which can be considered as "localized surface contouring", are also examined in this study. This paper describes the experimental and numerical investigations on the flow fields around these two types of airfoils under steady-state flow conditions. The main objective of the paper is to show that the newly proposed surface contouring successfully reduces the profile loss of the cascade, while the tripping wires employed in this study failed to provide any promising results, regardless of the wise size or position. Measurements using pneumatic probe and hot-wire probe are carried out to obtain time-averaged velocity and fluctuating velocity profiles on the airfoil suction surface in a low-speed cascade in a similar manner with the study by Vera et al. [18], who verified the usefulness of results obtained through low-speed cascade testing. Numerical simulation based on LES using a commercial solver is also executed to enhance the understanding of the flow field.

2. Experimental Setup

2.1 Test Apparatus and Cascades

2.1.1 Cascade of base-type airfoils

The test apparatus in the present study was the same as that of the previous study [8], except the test airfoil with separation-controlling contour or device. Figure 1 shows the test cascade that consisted of seven base-type (no device) airfoils with its design solidity. This figure also shows the situation where the airfoil pitch was changed in order to reduce the solidity, as will be described in the following. Table 1 indicates the airfoil geometry and cascade configuration. Upstream air-bleed and relatively large aspect ratio of the airfoil (2.28) was expected to help in achieving two-dimensional flow condition at least in the mid-span region. The Zweifel factor of the base-type cascade was almost the same as that of the airfoil employed by Hoheisel et al.[24]. Pitchwise periodicity of the cascade was carefully established through the adjustment of the two guide plates downstream of the cascade, monitoring stagnation pressure distribution on the outlet measurement plane. Two instrumented brass airfoils were in the middle of the cascade to measure static pressure distributions around the blade surface. Each of the instrumented airfoils, Airfoil #3 and Airfoil #4 in Figure 2, had 30 pressure holes of 0.5mm diameter on its suction and pressure surfaces, respectively. Airfoil #4 was the airfoil whose suction surface boundary layer was measured by use of a single hot-wire probe.

The solidity of the cascade in this study was changeable simply by inserting plates into the in-between spaces of the neighboring airfoils, with no modification of airfoil geometry. The examined solidity was expressed in terms of relative solidity-reduction rate from the designed value. The solidity reduction rates RRS was defined as

$$RRS = 1 - \frac{\sigma}{\sigma_{base}} . \quad (1)$$

The test case of $RRS = 14.2\%$ is designated S-15 hereafter and sometimes referred to as HL (High-Lift) condition. The other test cases were carried out for $RRS = 18.9\%$ and 23.6% , which are called S-20 or HL2 (Higher-Lift) and S-25 or UHL (Ultra High-Lift), respectively. The corresponding Zweifel factors for HL and UHL conditions were 1.14, 1.20 and 1.23 times of the designed condition, respectively.

2.1.2 Cascades of airfoils with device

Figure 2 shows the test airfoil with 2D contouring as separation-controlling device. The device is a kind of back-facing small step with gradual slope at the windward side and steep slope at the leeward side. As shown in this figure, this device was created by the modification of the front half of the suction surface of the base-type airfoil, while the pressure surface and the chord length were unchanged. The highest part of the contoured surface appeared before the flow over the suction surface reached the maximum, forming back-facing step-like shape there. The shape of this contouring was determined through some numerical calculations using MISES, a two-dimensional viscous/inviscid solver developed by Drela, which can deal with natural and bypass transitions. In consideration of the fact that only the center airfoil, the airfoil in the position Airfoil #4 of Figure 1, was mainly examined, only the middle three airfoils in the cascade were those with the 2D

contouring, where great attention was paid to the periodicity at least among the three. Besides, only the center airfoil was provided with 23 pressure holes on the suction surface, where the positions of the pressure holes are also depicted in Figure 2.

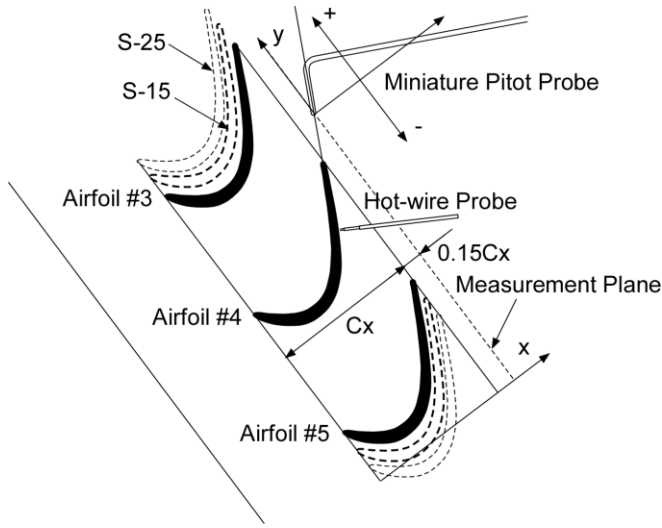


Figure 1 Test cascade composed of base-type airfoils (design and two reduced solidity cases)

Table 1 Airfoil geometry and cascade configuration

Chord length C	114mm
Axial chord length C_x	100mm
Span	260mm
Pitch t	variable
Inlet flow angle β_1	47deg
Outlet flow angle β_2	-60deg

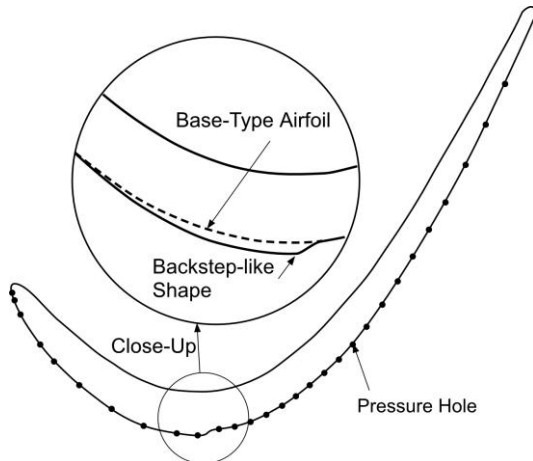


Figure 2 Test airfoil with 2D contouring, showing the positions of pressure holes

Figure 3 is the base-type airfoil with the 2D tripping wire (or bar) glued on the suction surface at five different positions. Likewise in the case of 2D contoured airfoil, the middle three airfoils were equipped with the tripping wires with the aid of cover tape pasted on the surface, as illustrated in Figure 4, where two instrumented base-type airfoils were at the positions of Airfoil #3 and Airfoil #5 sandwiching the airfoil to be measured. Since the same

instrumented base-type airfoils were again used here, some pressure holes were masked by the cover tapes and could not be used to monitor the pressure. The diameter of the wire d employed was 0.5 mm, 1 mm, 1.5mm and 2.8 mm.

2.2 Instruments

Static pressure distributions around the airfoil $p(x)$ were measured with a high-precision pressure transducer. The static pressure coefficient was calculated by

$$C_p(x) = (P_{01} - p(x)) / \left(\frac{1}{2} \rho \bar{U}_2^2 \right), \quad (2)$$

where P_{01} was the inlet stagnation pressure measured at the place 72 mm upstream of the leading edge of the center airfoil. The midspan cascade loss, defined by

$$Y_p(y) = \frac{P_{01} - P_{02}(y)}{\frac{1}{2} \rho \bar{U}_2^2}, \quad (3)$$

was obtained using two miniature Pitot probes (or Pitot-Static tube) whose head and total-pressure hole diameters were 3mm and 1.5 mm, respectively. The downstream Pitot probe was placed 15 mm downstream of the trailing edge of the airfoils in the axial direction. The probe head was aligned with the exit flow direction from the cascade for each of the measurements with the aid of flow observation using a tuft. A PC-controlled traversing unit automatically moved the probe along the measurement plane over two pitches with the positioning precision less than ± 0.05 mm.

Detailed boundary layer measurements using a single hot-wire probe were also conducted. The measurement area extended from $x/C_{ax} = 0.5$ to the blade trailing edge in the streamwise direction and from $y_n = 0.2$ mm to 10mm in the direction normal to the blade suction surface. A probe positioning machine enabled the automatic and precise probe movement along the normal lines to the airfoil surface. The velocity signal detected by a single hot-wire probe (Dantec 55P11) along with the CTA (Constant Temperature Anemometer, Kanomax) unit was then acquired by an A/D converter with sampling frequency of 20kHz. The size of each of the realizations, N_d , was 2^{13} word. Note that the air temperature was also measured by a thermocouple in order to compensate the measured data for temperature drift.

From these velocity data, u_k ($k = 1, \dots, N_f$), time-averaged velocity \bar{u} were calculated by the following equations.

$$\bar{u}(x, y_n) = \frac{1}{N_d N_f} \sum_{k=1}^{N_f} \sum_{j=1}^{N_d} u_k(x, y_n; j \Delta t), \quad (4)$$

where Δt was the data sampling interval ($= 50 \mu s$), N_f was the number of the realizations used for ensemble averaging ($= 20$). The outer edge of the boundary layer in this study was defined as the location where the time-averaged streamwise velocity reached 98% of the maximum velocity U_{ref} attained on the measurement line normal to the surface. The velocity fluctuation was calculated by

$$RMS(x, y_n) = \frac{1}{N_f} \sum_{k=1}^{N_f} \sqrt{\frac{\sum_{j=1}^{N_d} (\bar{u}(x, y_n) - u_k(x, y_n; j \Delta t))^2}{N_d}}. \quad (5)$$

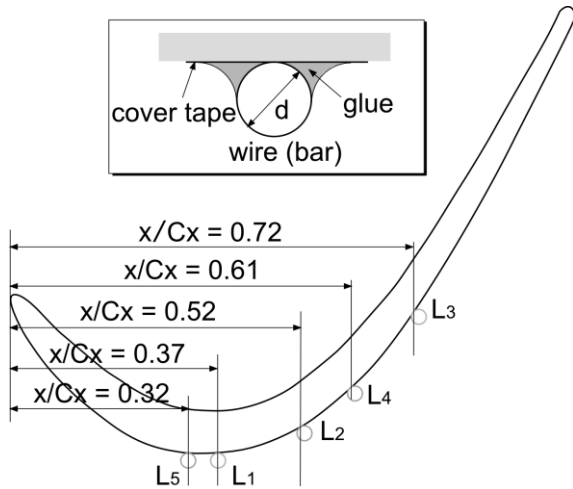


Figure 3 Test airfoil with tripping wire (bar) on the suction surface, showing the bar positions (bar diameter is 2.8 mm)

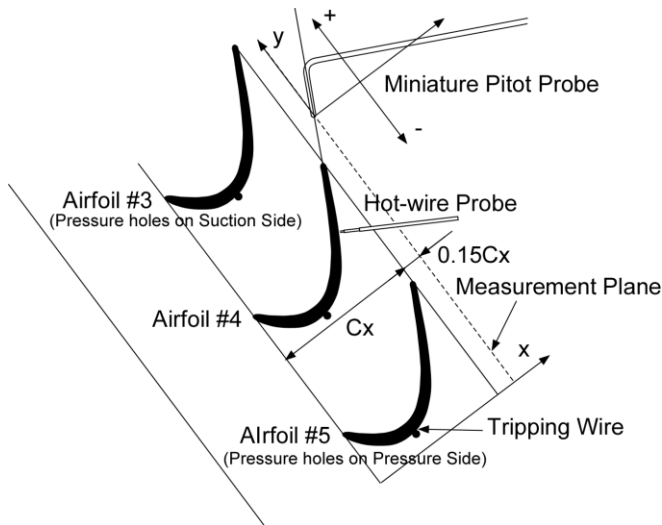


Figure 4 Test airfoils with tripping wire (bar) on the surface

2.3 Test Conditions

This study examined the flow fields with the exit Reynolds number $Re_2 = 5.7 \times 10^4$, 10×10^4 and 17×10^4 where the Reynolds number was defined as follows,

$$Re_2 = C\bar{U}_2/\nu, \quad (6)$$

where \bar{U}_2 is the averaged exit velocity. Inlet turbulence intensity was about 0.8%.

2.4 Uncertainty Analysis

Uncertainties associated with the pneumatic probe and hot-wire probe measurements were already reported in the previous study [26]. The most severe test condition for the pneumatic probe measurement in terms of the accuracy was the lowest speed flow condition ($U_{in} = 4.9\text{m/s}$) because of its very low dynamic pressure. Since the accuracy of the pressure transducer was $\pm 0.5\text{Pa}$, it was found from the standard procedure [25] that the uncertainty of the static pressure coefficient (Eq. (2)) was $\pm 3.5\%$ around the suction peak region of the coefficient. The uncertainty of the loss coefficient defined by Eq. (3) was about $\pm 7\%$ around the center of the wake.

Besides, the accuracy of the hot-wire probe measurement, which was mainly determined by the probe

calibration process using the Pitot probe, was estimated to be about $\pm 2\%$.

3. NUMERICAL SIMULATION

3.1 Flow Solver

The flow solver used in this study is a commercial software, ANSYS CFX 11. Large-Eddy Simulation (LES) using dynamic Smagorinsky subgrid scale model (DSM) was mainly used, while time-averaged Reynolds-Averaged Navier-Stokes (RANS) approach using Shear-Stress Transport (SST) two-equation model was also employed, occasionally along with a transition model ($\gamma - Re_\theta$), to grasp an image of time-averaged flow field concerned or to obtain an initial solution for the LES analysis. The second-order central difference scheme was used in space and the second-order backward scheme was employed in time. To make the analysis as time-accurate as possible, inner calculations during one time-step were repeated for 10 times at the maximum.

3.2 Computational Grids

Figure 5 is an example of the computational grids used in this code, which was for the flow analysis of the 2D contoured airfoils with HL (S-15) condition. The spanwise extent of the computational domain was $0.15 C_x$. The grid system consisted of several blocks to ensure the grid quality in terms of orthogonality on the airfoil surface and density near the surface as high as possible, where y^+ of the nearest grid point was less than 0.3 for $Re_2 = 5.7 \times 10^4$ case. Total number of the grid points in this case was about 7.5 millions with 50 equally-spaced grid points in the spanwise direction, making streamwise and spanwise spacings of the grids to be about 8 and 7 in wall unit, respectively.

3.3 Boundary Conditions

All flow quantities on the inlet boundary except inlet turbulence intensity were specified using the corresponding experimental data, while the mass flow rate was fixed on the outlet boundary. Periodic condition was applied in the pitchwise as well as spanwise directions as shown in Figure 5 and non-slip condition was specified on the airfoil. Courant number was about 1 for the LES analysis.

3.4 Code Validation

Figure 6 shows the static pressure coefficient distribution around the base-type airfoil for UHL condition calculated by the LES, in comparison with the measured data on the suction surface. The experimental data exhibits the occurrence of large-scale separation on the suction surface, followed by its transition and reattachment. It appears that the present LES simulation successfully reproduced the experimental static pressure distributions even for the highest loading condition, while the characteristics of the separation bubble was not properly captured by RANS simulation with the transition model implemented in the flow solver, as shown in the previous study [11]. Besides, slight difference can be identified around the reattachment zone, which was probably due to the fact that the inlet freestream turbulence was not taken into account in the analysis. Despite this difference, DSM-based LES analysis employed in this study seems to be able to provide more reasonable and detailed flow information than RANS simulation.

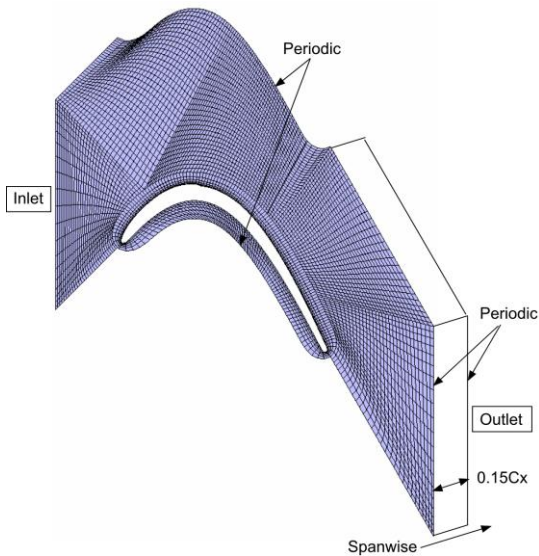


Figure 5 Grid system for the airfoil with 2D contouring, with every 5th grid lines depicted

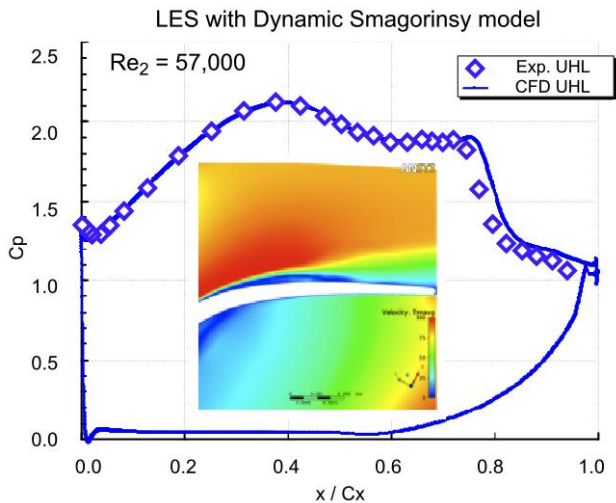


Figure 6 Static pressure distribution calculated by LES with dynamic Smagorinsky model, compared with the experiment of the base-type airfoil for UHL condition.

4. RESULTS

4.1 Effect of Tripping Wire

Before the investigation of effects of 2D contouring of the airfoil suction surface, pneumatic measurements were carried out to confirm how a tripping wire on the suction surface works as rather a conventional way to suppress the separation bubble.

Figure 7 shows static pressure distributions around the airfoils equipped with different size of the tripping wire fixed at the location L_2 ($x/C_x = 0.52$) including the distribution for no wire condition, where the tested cascade solidity corresponded to RRS-20% (higher loading condition) and the exit Reynolds number was 57000. It is clear that the wire with less than or equal to 1.0mm diameter did not make any large change of the static pressure distribution upstream of the wire, while the C_p downstream of the wire exhibited an abrupt increase probably due to the flow separation at the top of the wire. The wire with 1.5 mm or larger diameter caused marked decrease in C_p in front

of the wire due to its blockage effect, at the same time the wire induced C_p increase behind the wire. It can be concluded that the application of tripping wire was effective in suppressing the separation bubble that existed on the suction surface for no wire condition, whereas another large-scale separation was induced by the wire. It seems rather surprising to see that even the smallest wire in this experiment left some impact on the static pressure on the airfoil. Figure 8 illustrates the cascade loss distributions measured at the downstream of the airfoils. The wire with 1.5 mm or larger diameter considerably increased the cascade loss, while the wire with 1.0mm or smaller diameter did not bring about any notable difference in the loss distribution. This implies that although the application of small wire can be useful to suppress separation bubble, the aerodynamic penalty associated with the wire may cancel its benefit.

The findings in Figures 7 and 8 were obtained only in the case in which the wire was glued at the location L_2 . The loss coefficient was normalized with a reference loss coefficient. Further measurements were executed to examine the effect of the wire location on the static pressure and the cascade loss, as shown in Figures 9 and 10. The wire diameter was 1.5mm in this investigation, which was because this wire was found to have some noticeable influence on the cascade loss, at the same time, in consideration of actual scale of the test airfoil it was quite difficult to create a special device of this or smaller size on the airfoil by precision casting technique. Figure 9 indicates that the static pressure distribution was considerably affected by the wire location in different ways depending on the location. It was found that the wire at the region like L_1 or L_5 where the flow was still experiencing acceleration induced large pressure variation and the separation bubble observed at no wire condition was accordingly eliminated. However, as seen in Figure 10, the wire at L_1 or L_5 led to serious increase in the cascade loss. As the wire location moved toward the downstream (L_2 or L_4), the wire impact tended to be moderate. Interestingly enough, the wire at L_3 left only slightest influence on the static pressure and the cascade loss distributions. This was probably because the wire at L_3 ($x/C_x = 0.71$) was submerged in the separation bubble.

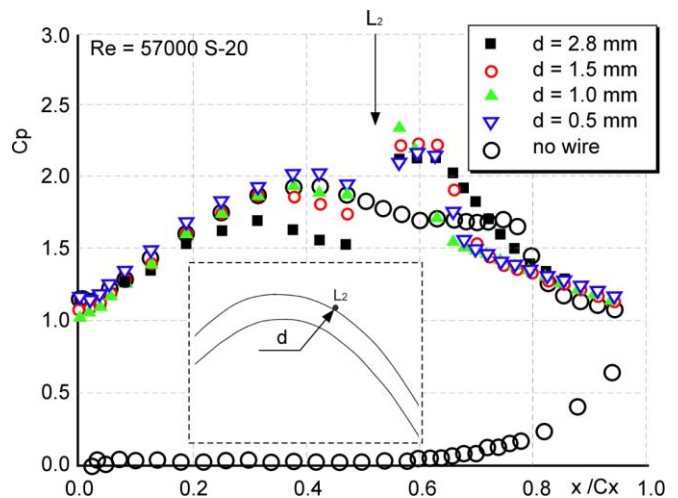


Figure 7 Effect of tripping wire diameter upon static pressure distributions around the airfoils equipped with tripping wire at the location L_2 ($Re_2=57000$, S-20)

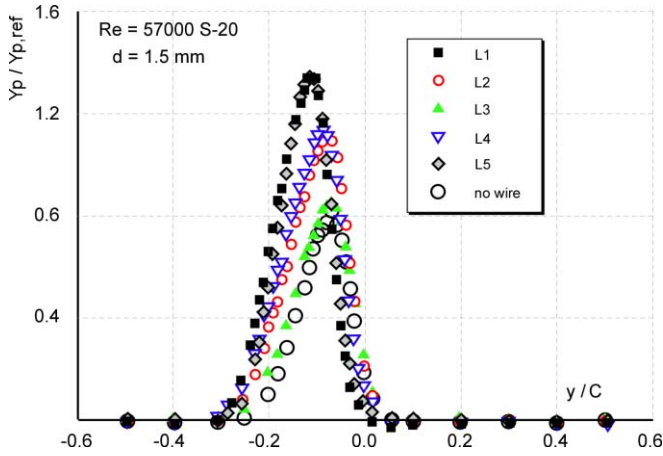


Figure 8 Cascade loss distributions measured at the downstream of the airfoils equipped with tripping wire at various locations ($Re_2=57000$, S-20)

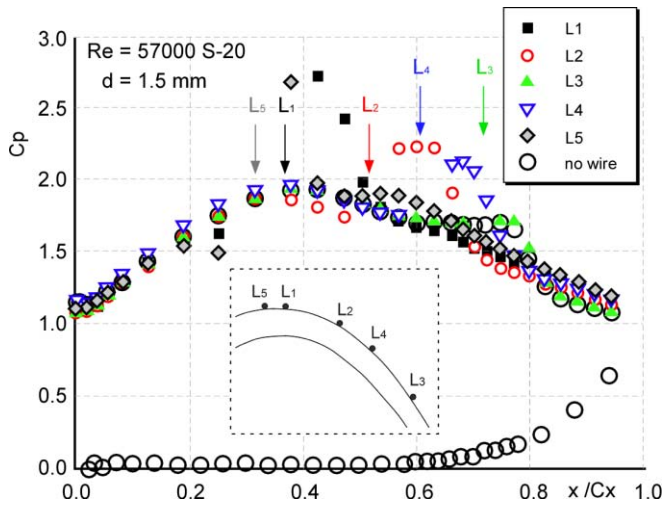


Figure 9 Static pressure distributions around the airfoils with tripping wire at various locations ($Re_2=57000$, S-20)

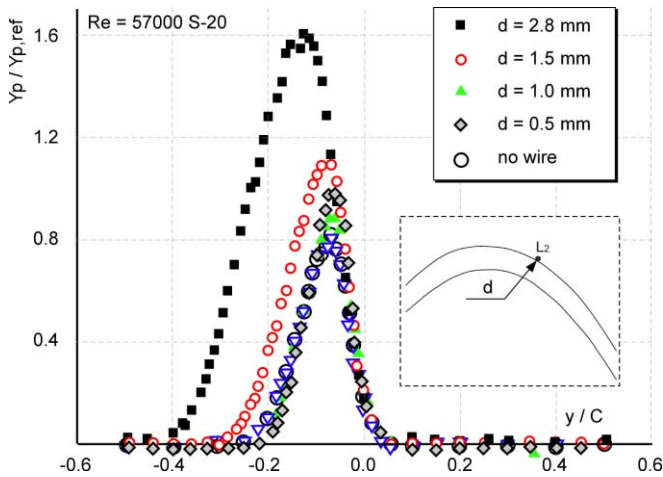


Figure 10 Effect of tripping wire diameter upon cascade loss distributions measured at the downstream of the airfoils with tripping wire at the location L_2 ($Re_2=57000$, S-20)

4.2 Effect of 2D-Contouring

4.2.1 Experimental Findings

Figure 11 shows the static pressure coefficient distributions of base-type and 2D-contoured airfoils measured under HL and UHL conditions, where $Re_2=57000$. This figure shows that UHL condition increased aerodynamic loading in comparison with HL condition. As for the base-type airfoil, both HL and UHL conditions

induced separation and reattachment on the suction surface, where the separation, transition and reattachment points for UHL condition happened earlier than for HL condition. When 2D-contouring was applied to the base-type airfoil, the values of C_p slightly increased due to the flow acceleration as shown in the close-up 1 of Figure 11. After the peaks appeared at about $x/C_x = 0.35$, the static pressure distributions on the 2D contoured airfoil decreased and tended to follow those of the base-type airfoil. It is also evident from Figure 11 that the separation bubbles observed for HL and UHL conditions were suppressed to a great extent. This observation can be confirmed by Figure 12, which comparatively shows time-averaged velocity magnitude contours measured for base-type and 2D-contoured airfoils under HL condition. Note that the velocity was normalized by the edge velocity of each streamwise measurement location. These contours have revealed that the introduction of 2D contouring almost completely eliminated the separation bubble. Figure 13 depicts the cascade loss distributions measured at the measurement plane located 15% C_x downstream of the airfoil trailing edge, where the position of y/t was the intersection between the measurement plane and the line from the target airfoil trailing edge along the designed flow direction. Figure 13 shows that the increase in airfoil loading induced additional cascade loss and the shift of the loss peak positions from the suction of Airfoil #4 to the pressure side of Airfoil #5, the latter implying a reduction of flow turning. The application of 2D contouring, irrespective of the loading level, reduced the cascade loss especially on the suction side of the airfoil, while the peak value and the pressure side loss distribution was nearly unchanged. This favorable result of the surface contouring technique was expected because some part of the loss appearing on the suction side of the airfoil wake was due to the separation bubble and abrupt growth of the boundary layer after the reattachment of the separation bubble.

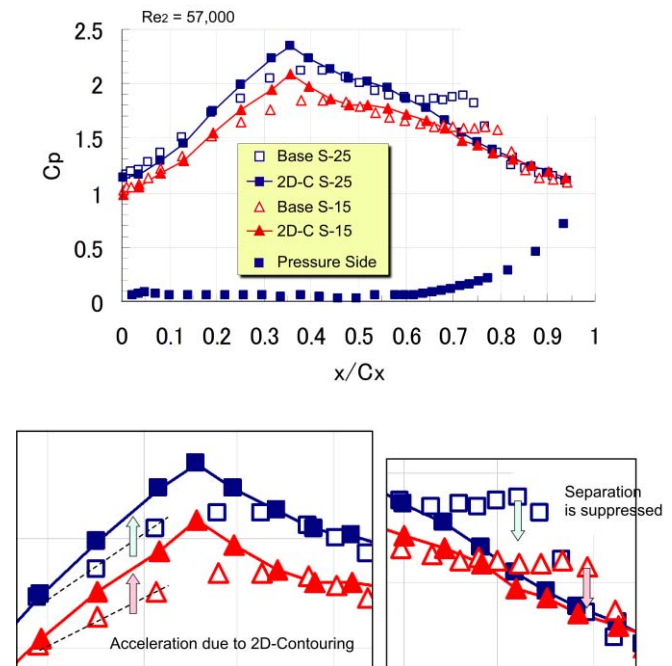


Figure 11 Static pressure distributions of base-type and 2D-contoured airfoils for HL and UHL conditions, with some close-up views ($Re_2=57000$)

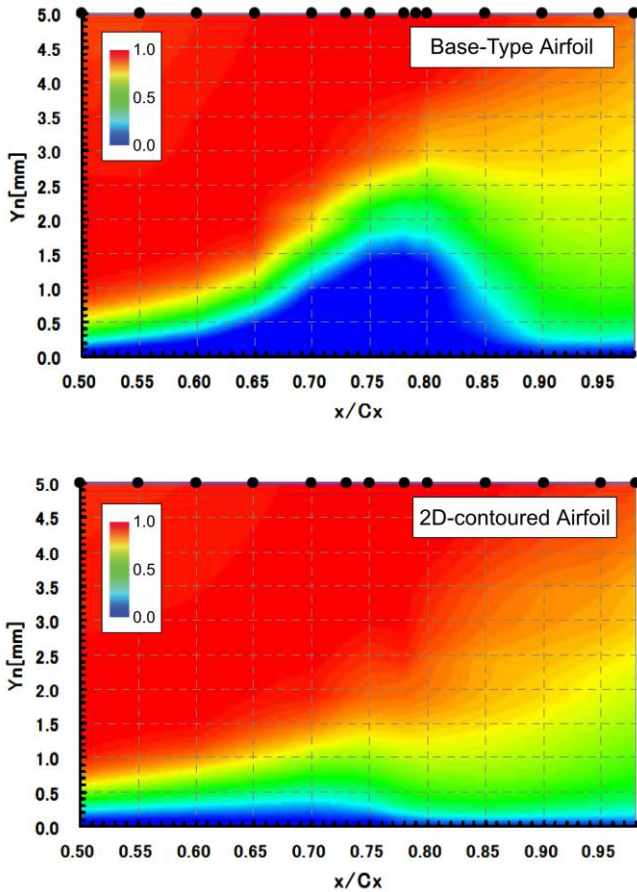


Figure 12 Time-averaged velocity magnitude contours measured for base-type airfoil (upper) and 2-D contoured airfoil (bottom) under HL loading condition ($Re_2=57000$)

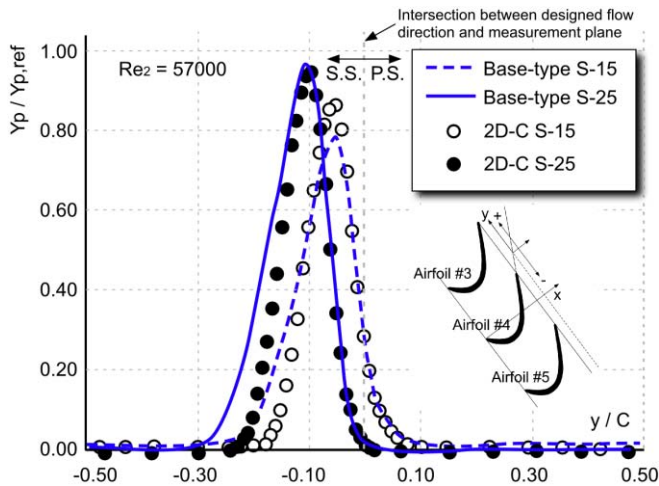


Figure 13 Cascade loss distributions measured at the downstream of base-type and 2D contoured airfoils for HL and UHL loading conditions ($Re_2=57000$)

4.2.2 Investigation on Flow Mechanism

In this section, some discussion will be made using experimental as well as numerical data to reveal what was actually happening over the surface of 2D-contoured airfoil so as to suppress separation bubble with no aerodynamic penalty, which was quite different from the cases using a tripping wire. Before the discussion, the capability of the flow solver was again checked by the comparison between the measured and calculated static pressure distributions around the base-type and 2D-contoured airfoils under HL condition. As shown in Figure 14, the flow calculation

using LES matched the measured data even for the 2D-contoured airfoil reasonably, which eventually gave the authors some confidence in the usage of the flow solver to enhance the understanding of the flow field. Nevertheless, since the calculation failed to capture the transitional behavior of the separation bubble, especially in the base-type airfoil case, which was mainly because free-stream turbulence was not taken into account in the calculation likewise in the case of Figure 6, some caution should be exercised in interpreting the numerical data.

Figure 15 shows velocity fluctuation contours obtained for base-type and 2D-contoured airfoils. The upper figure of Figure 15 contains a dashed curve showing an approximate position of the center of the shear layer, which nearly corresponded to the position on which local non-dimensional velocity magnitude was 0.5. The same data were reconstructed in a body-fitted coordinate system as shown in Figure 16, which is more useful to have better and accurate understandings of the transitional behavior of the boundary layers on the base-type and 2D-contoured airfoils. On the base-type airfoil surface, highly fluctuating region (high rms region) gradually emerged at about $x/C_x = 0.60$ and grew along the center of the shear layer of the separation bubble, followed by rapid increase in the value of rms due to transition onset of the shear layer occurring at about $x/C_x = 0.80$. It can be stated that the growth of velocity fluctuation along the shear layer center line was due to the effect of KH instability of the shear layer, which was followed by roll-up of the shear layer and vortex shedding from the rear end of the bubble, leaving large-scale high-amplitude velocity fluctuation there. This statement is supported by the theory of Chandrasekhar [28] and the results from FFT analysis of the velocity data obtained at the positions where the velocity fluctuation became the maximum for each of the streamwise measurement locations, as shown in Figure 17. This figure also exhibits the power spectrum of the calculated unsteady velocity data obtained at $x/C_x = 0.55$ only for 2-D contoured airfoil.

Power spectra of the velocity data measured over the base-type airfoil surface are shown on the top of Figure 17, with sharp peaks appearing at 371Hz. According to Chandrasekhar [28], K-H instability wave can happen when the following condition is met,

$$0 < kh < C, \quad (7)$$

where k is the wave number of instability wave and h is the characteristic length of the shear layer. The constant C is the upper limit of unstable region of K-H instability, which is 1 for a tanh-like velocity profile that could be a good approximation to a velocity profile within a separation bubble. From Eq. (7), the instability wave can appear with the following range of frequency f_{shear} ,

$$0 < f_{shear} < \frac{1}{2\pi} \frac{U_{shear}}{h}, \quad (8)$$

where U_{shear} is the phase velocity, which can be approximated by a half of the freestream velocity. Using the maximum height of the shear layer observed as $h (\cong 2\text{mm})$, it turns out as follows,

$$0 < f_{shear} < 398. \quad (9)$$

Since the theory in [28] predicts that the upper limit of f_{shear} in Eq. (9) corresponds to the maximum amplification rate of K-H instability, the wave with the frequency of about 400Hz is very likely to appear in the measurement, which matches the present observation ($f = 371\text{Hz}$).

On the contrary, the rms contours in the bottom of Figure 15 indicates that the boundary layer on the 2D-contoured airfoil contained highly fluctuating region near the airfoil surface before entering the measurement zone, which is designated Peak 1. In addition, there appeared another peak at a slightly distanced position from the wall, designated Peak 2. Then a large-scale highly fluctuating region emerged near the surface ranging from $x/C_x = 0.65$ to $x/C_x = 0.85$. Interestingly, the area where the velocity fluctuation existed almost corresponds to that where the separation bubble would have appeared for the base-type airfoil case. Since this velocity fluctuation region was analogous to that of the base-type airfoil, it is possible to think that the region was induced by vortex-related phenomena happening there.

It is clear from the Figure 17 (bottom) that two peaks appear at about 370 Hz and 600Hz in the power spectra of the measured velocity. The power spectrum of the numerical data is similarly characterized by the peaks occurring near 370 Hz and 600Hz, accompanied by another peak at about 250Hz. Despite a limited number of FFT-analyzed numerical data and the appearance of the peak at 250Hz, it seems that the LES analysis was able to capture an important feature of the flow field to some extent. Figure 18 shows some snapshots of velocity fluctuation in rms around the 2D-contoured airfoil under HL loading condition for $Re = 57000$ and Figure 19 is the contour of time averaged velocity fluctuation time-averaged flow fields, which corresponds to the measured contour shown on the right of Figure 16. As can be seen in Figure 14, there remains a small separation bubble in the calculation. Figure 18 indicates that the region of high velocity fluctuation starts to appear just behind the rear end of the surface contouring, being convected almost along the airfoil suction surface towards the trailing edge. The rms value in the high fluctuating region gradually increases in the streamwise direction with the peak happening over the area from $x/C_x = 0.60$ to $x/C_x = 0.65$, designated A1 in Figure 18. This peak region seems to be the counterpart of Peak 2 in Figure 15. The peak region exhibits some instability after $x/C_x = 0.65$, then rolling-up into a vortex-like structure designated A2 at $x/C_x = 0.70$. The highly fluctuating region as shown in the bottom of Figure 15 can be attributed to this vortex-like structure. Since the velocity at $x/C_x = 0.55$ does not seem to be under the direct influence of the vortex-like structure, it can be inferred that the peak at 600Hz was closely related to the vortex movement, while the peak appearing at 370Hz was possibly associated with the unsteady behavior of the highly fluctuating region that originated from the end of the surface contouring.

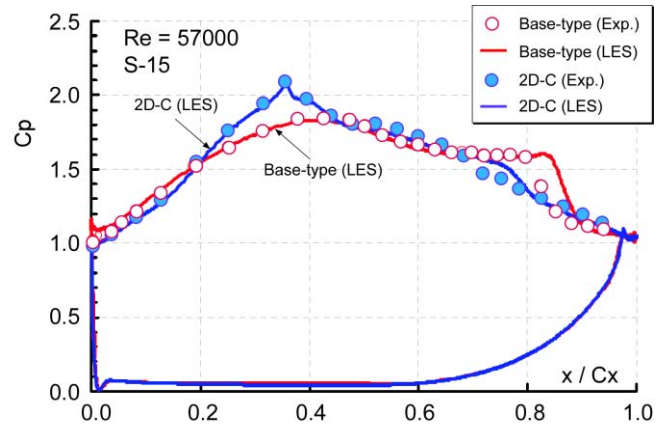


Figure 14 Comparison of static pressure distribution between the measurements and LES predictions under HL condition

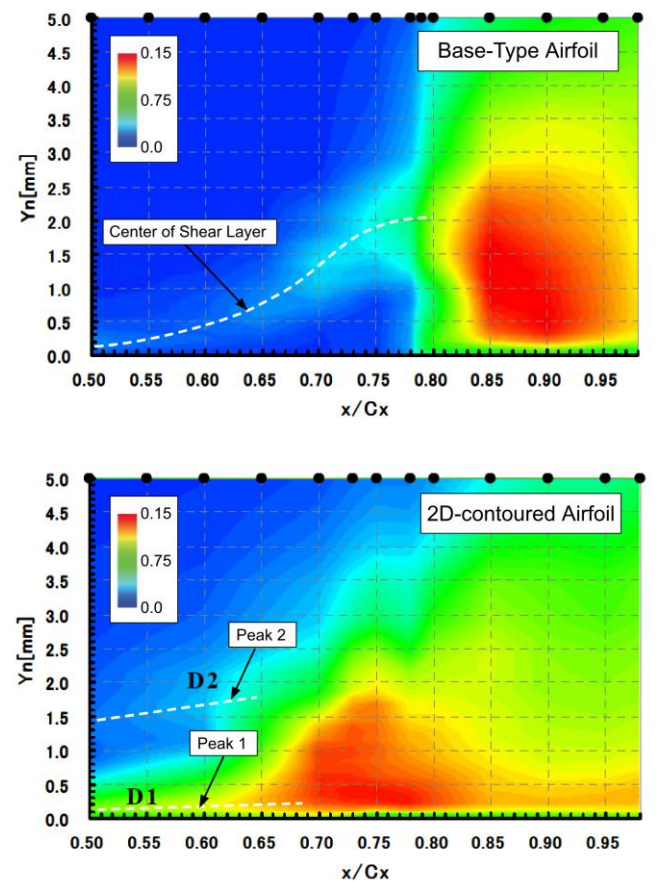


Figure 15 Time-averaged velocity fluctuation (rms) contours measured for base-type airfoil (top) and 2-D contoured airfoil (bottom) under HL loading condition ($Re_2=57000$)

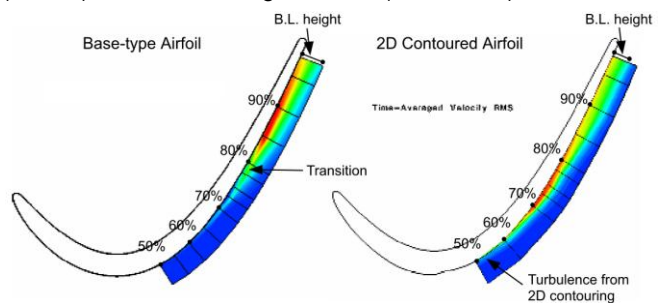


Figure 16 Time-averaged velocity fluctuation (rms) contours measured for base-type airfoil (left) and 2-D contoured airfoil (right), which are the same as those in Figure 15 but in a different way of expression

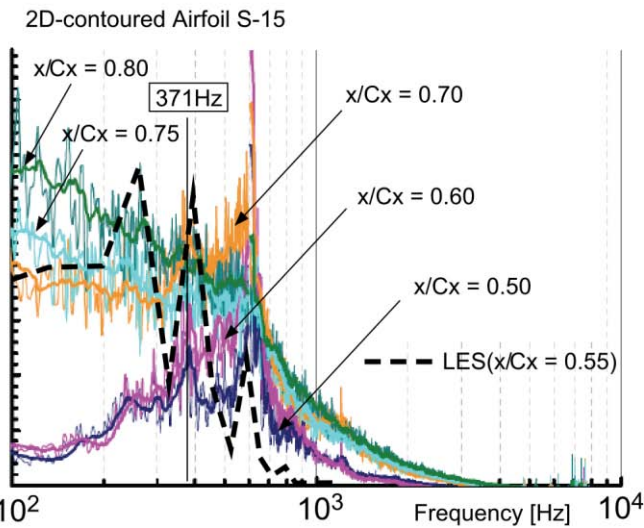
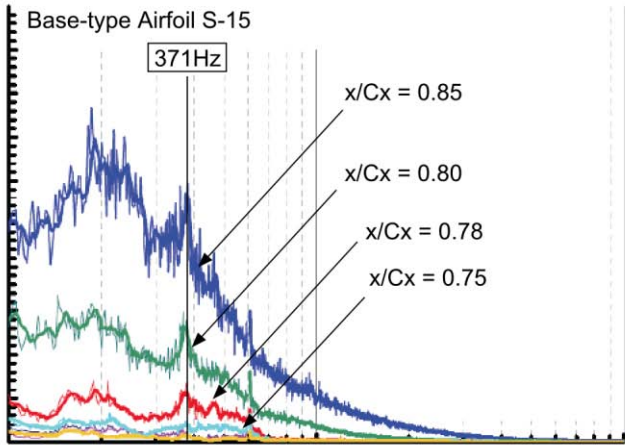


Figure 17 Power spectra of the velocity data obtained on the surfaces of base-type (top) and 2D-contoured (bottom) airfoils under HL loading condition ($Re=57000$)

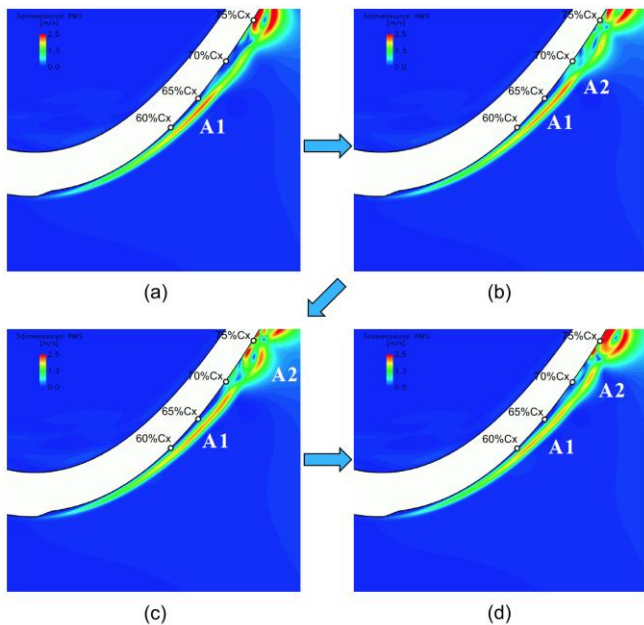


Figure 18 Some snapshots of calculated velocity fluctuation in rms around 2D-contoured airfoil under HL loading condition for $Re = 57000$

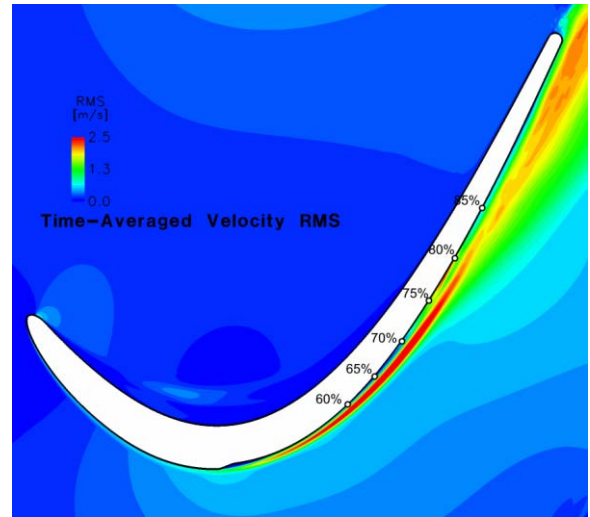


Figure 19 Contour of time-averaged velocity fluctuation (rms) around 2D-contoured airfoil calculated under HL loading condition for $Re = 57000$

4.2.3 Effect of Reynolds number

Figure 20 shows static pressure distributions on the base-type and 2D-contoured airfoils at three Reynolds numbers. It is clear that the separation bubble observed on the base-type airfoil disappeared for all cases with the application of 2D contouring. Note that small separation was identified just downstream of the rear end of the surface contouring at $Re = 170000$.

Figure 21 shows loss coefficients of the base-type and 2D-contoured airfoils plotted against the Reynolds number at HL and UHL loading conditions. Significant loss reduction was attained for both loading conditions at $Re = 57000$. For higher Reynolds number cases the effect of the surface contouring became obscure especially for HL condition, while some favorable impact was still confirmed for UHL condition. It can be also mentioned that the loss reduction trend against the Reynolds number for the 2D-contoured airfoil can be approximated by a curve of $Re^{-0.2}$, which implied that the boundary layer over the suction surface of the contoured airfoil was dominated by turbulent boundary layer, as expected from the other experimental data.

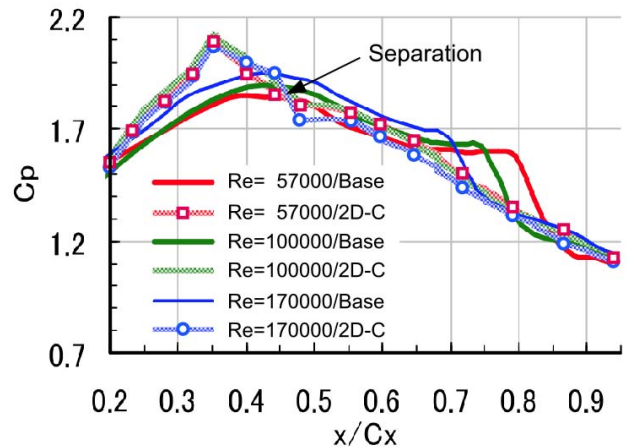


Figure 20 Static pressure distributions measured at three Reynolds numbers for base-type and 2D-contoured airfoils

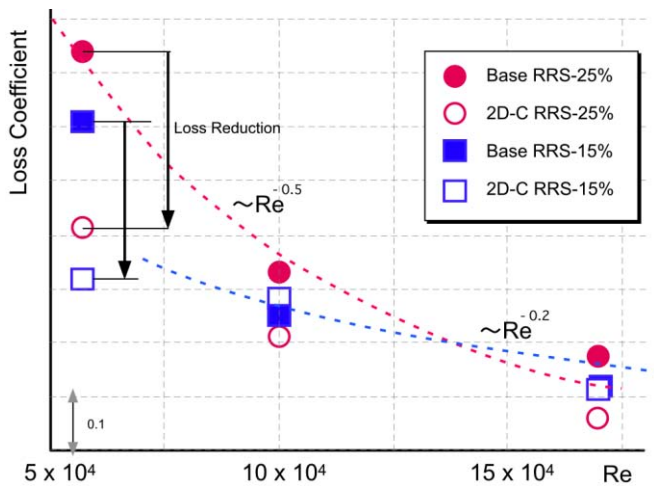


Figure 21 Variation of loss coefficient with Reynolds number for base-type and 2D-contoured airfoils

5. CONCLUSIONS

This study conducted detailed pneumatic probe and hot-wire probe measurements of the airfoil with special device on its suction surface, which was two-dimensional surface contouring, for various loading and Reynolds number conditions. The surface contouring was established by adding a kind of slope on the suction surface of the base-type airfoil. Large Eddy Simulation using dynamic Smagorinsky model as subgrid scale model was also carried out to enhance the understanding of the complicated flow field around the 2D-contoured airfoil. For the sake of comparison, the airfoil with a tripping wire was also examined.

While the tripping wire did not provide any benefits, it turned out from the detailed experiments and LES analysis that the 2D contouring of the airfoil suction surface was very effective for suppressing the separation bubble, resulting in significant improvement of cascade aerodynamic performance. Several efforts were made to understand the physics of the flow field over the contoured airfoil, indicating that the velocity fluctuation created behind the rear end of the contouring played an important role in suppressing the separation bubble. However, further studies are still needed to find out the mechanism in more detail.

ACKNOWLEDGMENT

The authors are greatly indebted to efforts made by K. Okamura in the preparation of the manuscript.

REFERENCES

- [1] Hodson, H. P., Huntsman, I. and Steele, A. B., 1993, "An Investigation of Boundary Layer Development in a Multistage LP Turbine," ASME Paper 93-GT-310.
- [2] Schulte, V. and Hodson, H. P., 1998, "Prediction of the Recalmed Region for LP Turbine Profile Design," *Trans. ASME Journal of Turbomachinery*, Vol. 120, pp. 839-846.
- [3] Stieger, R. D. and Hodson, H. P., 2003, "The Transition Mechanism of Highly-Loaded LP Turbine Blades," ASME Paper GT2003-38304.
- [4] Funazaki, K., Yamada, K., Ono, T., Segawa, K., Hamazaki, H., Takahashi, A. and Tanimitsu, H., 2006, "Experimental and Numerical Investigations of Wake Passing Effects upon Aerodynamic Performance of a LP Turbine Linear Cascade With Variable Solidity," ASME GT2006-90507.
- [5] Funazaki, K., Yamada, K., Chiba Y. and Tanaka N., 2008, "Numerical and Experimental Studies on Separated Boundary layers over Ultra-High Lift Low-Pressure Turbine Cascade Airfoils with variable Solidity: Effects of Free-stream Turbulence," ASME GT2008-50718.
- [6] MaAuliffe, B.R. and Yaras, M.I., 2010, "Transition Mechanisms in Separation Bubbles under Low- and Elevated Freestream Turbulence", ASME Journal of Turbomachinery, Vol. 132, January.
- [7] Zhang, X.F. and Hodson, H., 2010, "Freestream Turbulence Intensity on the Unsteady Boundary Layer Development on an Ultra-High-Lift Low Pressure Turbine Airfoil", ASME Journal of Turbomachinery, Vol. 132, January.
- [8] Michalek, J., Monaldi, M. and Arts, T., 2010, "Aerodynamic Performance of a Very High Lift Low Pressure Turbine Airfoil (T106C) at Low Reynolds and High Mach Number with Effect of Free Stream Turbulence Intensity", ASME GT2010-22884.
- [9] Howell, R. J., Ramesh, O.N., Hodson, H.P., Harvey, N.W., Schulte, V., 2000, "High Lift and Aft Loading Profiles for Low Pressure Turbines", *Journal of Turbomachinery*, Vol. 123, pp. 181-188.
- [10] Praisner, T.J., Grover, E.A., Knezevici, D.C., Popovic, I., Sjolander, S.A., Clark, J.P. and Sondergaard, R., 2008, "Toward the Expansion of Low-Pressure-Turbine Airfoil Design Space," ASME GT2008-50898.
- [11] Funazaki, K., Shiba, T, Tanimitsu, H., 2010, "Effects of Blade Loading Distributions on Aerodynamic Performance of Ultra-High Lift LP Turbine Airfoils under the Influence of Wake Passing and Freestream Turbulence", ASME GT2010-22134.
- [12] Corke, T.C. and Thomas, F.O., 2003, "Enhanced Design of Turbo-Jet LPT by Separation Control using Phased Plasma Actuators", NASA/CR-2003-212294.
- [13] Hultgren, L. and Ashpis, D.E., 2004, "Boundary-Layer Separation Control under Low-Pressure-Turbine Conditions using Glow-Discharge Plasma Actuators", NASA/TM-2004-212913.
- [14] Huang, J., 2005, "Separation Control over Low Pressure Turbine Blades using Plasma Actuators", Doctoral Dissertation, Notre Dame University.
- [15] Bons, J., Sondergaard, R. and Rivir, R.B., 2002, "The Fluid Dynamics of LPT Blades Separation Control using Pulsed Jets", ASME Journal of Turbomachinery, Vol. 124, January.
- [16] Gross, A. and Fasel, H.F., 2005, "Numerical Investigation of Low-Pressure Turbine Blade Separation Control", *AIAA Journal*, Vol. 43, 12, pp. 2514-2525.
- [17] Fernandez, E., Kumar, V., Kumar, R. and Alvi, F., 2010, "Active Separation Control on Highly Loaded LPT Blades using Microjets", AIAA Paper 2010-1119.
- [18] Vera, M., Zhang, X.F., Hodson, H. and Harvey, N., 2007, "Separation and Transonic Control on an Aft-Loaded Ultra-High-Lift LP Turbine Blade at Low Reynolds Numbers: High-Speed Validation", ASME Journal of Turbomachinery, Vol. 129, April.
- [19] Montis, M., Niehuls, R. and Flala, A., 2010, "Effect of Surface Roughness on Loss Behaviour, Aerodynamics

- Loading and Boundary Layer Development of a Low-Pressure Gas Turbine Airfoil”, ASME GT2010-23317.
- [20] Funazaki, K., Okuno, Y. and Yamada, K., 2007, “Studies on LP Turbine Blade Surface Roughness Elements for Controlling Separation Bubble to Improve Aerodynamic Performance of the Turbine Blades (in Japanese)”, Proceedings of 35th GTSJ Annual Meeting (Gifu)
- [21] Luo, H., Qiao, W. and Xu, R., 2009, “Passive Control of Laminar Separation Bubble with Spanwise Groove on a Low-speed Highly Loaded Low-Pressure Turbine Blade”, Journal of Thermal Science, Vol. 18, 3, pp.193-201.
- [22] Mathesis, B.D., Huebsch, W.W. and Rothmayer, A.P., 2004, “Separation and Unsteady Vortex Shedding from Leading Edge Surface Roughness”, Report of RTO AVT Specialist’s Meeting (Prague), RTO-MP-AVT-111.
- [23] Martinstetter, M., Niehuis, R. and Franke, M., 2010, Passive Boundary Layer Control on a Highly Loaded Low Pressure Turbine Cascade, ASME Paper GT2010-22739.
- [24] Hoheisel, H., Kiock, R., Lichtfuss, H.L. and Fottner, L., 1987, "Influence of Free-Stream Turbulence and Blade Pressure Gradient on Boundary Layer and Loss Behavior of Turbine Cascade," ASME Trans., Journal of Turbomachinery, Vol. 109, pp. 210-219.
- [25] Kline, S. J. and McClintock, F. A., 1953, "Describing Uncertainties in Single Sample Experiments," *Mechanical Engineering*, Vol. 75, pp. 3 - 8.
- [26] Funazaki, K., Yamada, K., Tanaka, N. and Chiba, Y., 2009, Detailed Studies on Separated Boundary Layers over Low-Pressure Turbine Airfoils under Several High Lift Conditions: Effect of Freestream Turbulence, ASME GT2009-59813.
- [27] Lan, J., Xie, Y., Zhang, D. and Shu J., 2009, Large-Eddy Simulation and Passive Control of Flows for a Low Pressure Turbine Cascade, ASME GT2009-59833
- [28] Chandrasekhar, S., 1981, Hydrodynamics and Hydromagnetic Stability, Clarendon, Oxford.